

Article

A Study on the Stoichiometry of Casein/Chitosan Gel Complexes as a Delivery System for Quercetin

Sofia Milenkova ¹, Nikolay Zahariev ^{2,3}, Rita Ambrus ⁴, Bissera Pilicheva ^{2,3} and Maria Marudova ^{1,*}

¹ Faculty of Physics and Technology, University of Plovdiv "Paisii Hilendarski", 24 Tsar Asen Str., 4000 Plovdiv, Bulgaria; sofia.milenkova@uni-plovdiv.bg

² Department of Pharmaceutical Sciences, Faculty of Pharmacy, Medical University of Plovdiv, 15A Vassil Aprilov Blvd, 4002 Plovdiv, Bulgaria; nikolay.zahariev@mu-plovdiv.bg (N.Z.); bissera.pilicheva@mu-plovdiv.bg (B.P.)

³ Research Institute, Medical University of Plovdiv, 15A Vassil Aprilov Blvd, 4002 Plovdiv, Bulgaria

⁴ Faculty of Pharmacy, Institute of Pharmaceutical Technology and Regulatory Affairs, University of Szeged, H-6720 Szeged, Hungary; ambrus.rita@szte.hu

* Correspondence: marudova@uni-plovdiv.net

Abstract: As a well-known plant flavanol, quercetin possesses a diverse range of biological properties. These include its ability to act as an antioxidant, reduce inflammation, and exhibit anticancer effects. Consequently, it finds extensive application in numerous models related to wound healing. However, the poor physicochemical characteristics of the molecule (which include low solubility, stability, and permeability) eventually reduce its bioavailability at the targeted sites. A variety of nano formulations with great therapeutic potential have been created in order to get around these obstacles on the way to successful therapy. The current investigation aims to examine the properties of nano- and micro-sized casein/chitosan gel polyelectrolyte complexes (PECs) with respect to their potential for quercetin loading and release. Four different types of hydrogel particles at pH 6 and different casein/chitosan charge ratios were synthesized; namely, 1:1, 2:1, 4:1, and 6:1 in excesses of casein. The attractive electrostatic interactions between the oppositely charged polyelectrolytes were proved by FT-IR spectroscopy. The process yield increased from 37.5% to 72.5% in excesses of casein. The gel particle's size varied between 377 nm and 5.72 μm depending on the casein/chitosan stoichiometry. The morphology of the obtained gel polyelectrolyte complexes was found to be spherical, based on scanning electron microscopy and atomic force microscopy analysis. The quercetin loading efficiency was above 95% for all investigated hydrogel complexes. Investigation of the physical state of the loaded polyphenol by the differential scanning calorimetry and X-ray powdered diffraction technique suggested the occurrence of partial recrystallization phenomena. The quercetin release test was performed in phosphate buffer (pH 5.5) at 32 °C and permanent stirring at 50 rpm. A zero-order model was used to describe in the best way the release kinetics. The reported casein/chitosan complexes loaded with quercetin may find application in wound healing as a concomitant treatment.

Keywords: polyelectrolyte gel complexes; casein; chitosan; drug delivery



Citation: Milenkova, S.; Zahariev, N.; Ambrus, R.; Pilicheva, B.; Marudova, M. A Study on the Stoichiometry of Casein/Chitosan Gel Complexes as a Delivery System for Quercetin. *Appl. Sci.* **2023**, *13*, 10868. <https://doi.org/10.3390/app131910868>

Academic Editor: Raed Abu-Reziq

Received: 7 September 2023

Revised: 25 September 2023

Accepted: 27 September 2023

Published: 30 September 2023



Copyright: © 2023 by the authors. Licensee MDPI, Basel, Switzerland. This article is an open access article distributed under the terms and conditions of the Creative Commons Attribution (CC BY) license (<https://creativecommons.org/licenses/by/4.0/>).

1. Introduction

As the biggest organ, it is important to keep the skin healthy and intact, so that it can protect the whole body from external traumas. In cases of injury or harm, especially ones damaging to its integrity in depth, the protective function of the skin as a barrier can be compromised. An appropriate treatment procedure should be applied, depending on the depth and the stage of the wound [1]. Sometimes, treatment plans can be extended up to 12 weeks. In cases where the wound is chronic, the healing process can be prolonged, and the wound spot becomes more susceptible to bacterial infections [2]. In most cases, in order to avoid the development of infections in and around the wound, the prescription of antibiotics is required, but the significant increase in the number of drug-resistant bacterium

types is increasingly/quite worrying [1]. A possible way out of this is to combine the existing antibiotic therapy with a biologically active compound that can prevent bacterial development. An appropriate candidate for this could be quercetin. This compound is naturally found in different fruits and vegetables and belongs to the flavanol group [3]. Along with its high antioxidant activity and biocompatibility, quercetin also shows antiviral, anti-inflammatory, anti-microbial, and even anti-carcinogenic properties [4,5]. It is able to downregulate proteins responsible for tumorigenesis and development and it can affect cell signalling and enzyme inhibition, according to Wendlocha et al. [6]. However, its treatment potential cannot be fully exploited due to its poor solubility. One of the often-chosen and effective methods for improving the compound is to encapsulate it into hydrogel particles. As a matter of fact, gel-based particles made of biopolymers are a suitable carrier for bioactive compounds with low solubility [7], low skin permeability [8], and poor in vivo behaviour [9]. Due to their high flexibility and biocompatibility, they have become an emerging tool for encapsulation and delivery of different types of active compounds, not only in the pharmacy industry, but also in medical skin care products [10], cosmetics [11], the food industry [12], etc. In addition, the overall synergistic outcome between the active compound and the gel cargo system is quite easy to achieve [13]. Gel particles are suitable for enhancing quercetin solubility and its delivery onto a desired spot on the skin. Esposito et al. have concluded that quercetin encapsulated into PVA–alginate hydrogels shows appropriate penetration in ex vivo skin models [14]. Hydrogels developed by Wang et al. [1] demonstrate proper mechanical resilience and water vapour transmission rate, along with a synergetic effect between the active compound and the matrix consisting of quaternized chitosan and polyacrylamide.

Besides its anti-microbial activities, chitosan also possesses other valuable features, such as mucoadhesion, biocompatibility, degradability, and lack of toxicity [15,16]. Along with this, chitosan hydrogels also show hemostatic, wound healing effects and anti-inflammatory actions [17]. Being a weak polyelectrolyte, when placed in conditions up to its pKa of ~6.5, at least 50% of the macromolecules of chitosan/macromolecules present in chitosan are positively charged. Thus, based on electrostatic interactions, it can form a variety of structures (hydrogel particles [18], thin films [19], multi-layered films [20], etc.) suitable for delivering active compounds for skin treatment.

Casein is a weak polyelectrolyte and protein with an isoelectric point at pH = 4.6. At higher pH levels, it is negatively charged [21]. Casein can form micelles in water conditions above its critical micellar concentration, and it possesses film-forming, gelling, and foaming properties. It is proven to be safe for biomedical applications due to its biocompatibility and biodegradability [22,23]. Also, it has both hydrophobic and hydrophilic domains and can interact with various compounds [24]. As casein and chitosan are oppositely charged at pH = 6, they are suitable complexing/complex-forming partners. Depending on the ratio between the active groups within the casein and chitosan structures, the resulting structures can form either stoichiometric water non-soluble complexes or non-stoichiometric water-soluble complexes in excess of one of the complexation partners [25].

In the present study, we examine the formation of gel particles of polyelectrolyte complexes between casein and chitosan at different stoichiometric ratios. The hydrogel particles are obtained through a gelation technique, followed by an ultra-sonication step. Their potential as quercetin delivery systems and the physico-chemical properties of the final structures are examined and shown herein.

2. Materials and Methods

2.1. Materials

Sodium salt of casein (CAS) (from bovine milk) and dialysis membranes were bought from Sigma Aldrich (St. Louis, MO, USA). Chitosan with low molecular weight with fungal origin (CH) was provided by Glentham life sciences (Corsham, UK). Based on the producer's product specification, its viscosity (1% chitosan in 1% acetic acid solution at 20 °C) varies between 10 cps and 120 cps. The degree of deacetylation is $\geq 85\%$. Quercetin

dihydrate 97% with molecular weight 338.27 g/mol was ordered from Thermo Scientific Chemicals (Waltham, MA, USA). Other solvents and low-molecular-weight salts were used with analytical grades of purity. Adrona Crystal B30 Bio was used for Ultra-pure water purification with a conductivity of 0.055 $\mu\text{S}/\text{cm}$.

2.2. Methods

2.2.1. Preparation of Casein/Chitosan Nanocomplexes

Casein/chitosan complexes were formed by using ionotropic gelation based on the attractive electrostatic interactions between the oppositely charged polyelectrolytes. First, 0.5% w/v of water solution of casein (pH = 7) and 0.5% w/v solution of chitosan in 3% acetic acid were left to stir during the night to achieve complete solubility. Prior to the mixing step, the pH value of the solution of chitosan was increased to 5 by 5 M NaOH. The complex formation occurred after mixing different volumes of polyelectrolyte solutions, thereby achieving theoretical stoichiometric ratios between their charged groups, $\text{COO}^-/\text{NH}_3^+$ (namely, 1:1, 2:1, 4:1, and 6:1 in favour of casein). The total amount of the reaction mixture is always constant and equal to 20 mL. Immediately after the mixing step, the pH of the resultant solution was adjusted to pH = 6 and left to stir for 15 min at room temperature and 1500 rpm. After this, the solutions were ultrasonicated in an ice bath at an amplitude of 90% for 20 min using the UP100H Compact Ultrasonic Laboratory Device (Hielscher Ultrasonics GmbH, Teltow, Germany). The same preparation protocol was followed for the quercetin-loaded particles. First, 50 mg of quercetin was dissolved in 3.5 mL of ethanol and added to the chitosan solution before the complex formation step. The obtained structures were precipitated at 14,000 rpm for 15 min and lyophilized for 72 h at 10 Pa pressure and a temperature of $-50\text{ }^\circ\text{C}$. The final dry mass was sealed in containers and stored at controlled humid conditions (RH 54%) at room temperature for further applications.

2.2.2. FTIR Spectroscopy

AVATAR 330 FT-IR spectrometer (Thermo Nicolet, Thermo Fisher Scientific Inc., Waltham, MA, USA) equipment was used to study the interactions between the polyelectrolytes and confirm the presence of the active compound. Each sample was mixed with 150 mg of dry KBr in a mortar made of achate. Afterwards, this mixture was prepared as a tablet using a hydraulic press Specac[®] (Specac, Inc., Orpington, UK) with a 10 ton pressing force. The spectra were obtained in the region of 4000 and 400 cm^{-1} , with 4 cm^{-1} resolution. The OMNIC[®] software package (Version 7.3, Thermo Electron Corporation, Madison, WI, USA) was used for data curation and analysis.

2.2.3. Size Polydispersity of Casein/Chitosan Nanocomplexes

Sizes and histograms of the volume distribution of the obtained complexes were examined through the dynamic light scattering technique using a Nanotracc particle size analyser (Microtrac, York, PA, USA).

The width of the size distribution for the investigated systems was calculated using the given formula:

$$\text{Span} = \frac{v(90\%) - v(10\%)}{v(50\%)} \quad (1)$$

where $v(90\%)$ —90% of the volume distribution is below this value; $v(10\%)$ —10% of the volume distribution is below this value; and $v(50\%)$ —the volume median diameter is the diameter where 50% of the distribution is above and 50% is below.

2.2.4. Morphology of Casein/Chitosan Nanocomplexes

Scanning electron microscopy (SEM) (Prisma E SEM, Thermo Scientific, Waltham, MA, USA) was used to examine the shape, size, and aggregation phenomena of the nanocomplexes. A couple of milligrams of the structures were fixed onto a holder of copper and coated with carbon and gold subsequently using a vacuum evaporator (BH30, Prisma E SEM, Thermo

Scientific, Waltham, MA, USA). The resultant photos were recorded using a back-scattered electrons detector (Prisma E SEM, Thermo Scientific, Waltham, MA, USA) at 15 kV.

The morphology of the gel particles was further investigated using atomic force microscopy (AFM) (Nanosurf FlexAFM (Nanosurf AG, Liestal, Switzerland)). The particles were homogenized in pure water and this dispersion was dripped onto a clean microscopic glass. A minute after this, the surface was lightly washed with distilled water and left to dry until the next day. The AFM microphotographs were performed in a tapping regime using a standard cantilever Tap190Al-G (Nanosurf AG, Liestal, Switzerland) with a radius of the tip of 10 nm. The resultant photographs were collected for a 0.7 s scan time for each line with a viewing field of 256×256 pixels and showing a $10 \times 10 \mu\text{m}$ area from the sample surface.

2.2.5. Yield and Loading Efficiency

The yield of the resultant structures was studied by measuring the weight of the lyophilized complexes, and it was calculated with the following equation:

$$\text{Yield (\%)} = \frac{\text{Mass of the lyophilized formulation}}{\text{Sum of the mass of dry components in the formulation}} \times 100 \quad (2)$$

After gel complex formation and the first centrifugation, the supernatant was taken out. The concentration of quercetin, unloaded in the supernatant, was calculated by measuring the supernatant extinction at 256 nm using a spectrophotometer Metertech SP-8001 (Metertech Inc., Nangang, Taipei, Taiwan) based on the preliminary prepared calibration curve. The amount of drug loaded into the dried gels was evaluated as:

$$\text{Loading efficiency (\%)} = \frac{m_0 - m}{m_s} \cdot 100 \quad (3)$$

where m_0 —the whole amount of Que; m —the mass of non-loaded Que measured spectrophotometrically; and m_s —the mass of the nanocomplex after lyophilization.

2.2.6. Thermal Stability and Phase State

The phase state and thermal stability of quercetin and empty and quercetin-loaded complexes were studied using the differential scanning calorimetry equipment DSC 204F1 Phoenix (Netzsch Gerätebau GmbH, Selb, Germany). All of the samples were closed hermetically in same type of aluminium pans. An identical empty pan was used as a control. The heating process proceeded at a heating rate of $10 \text{ }^\circ\text{K}/\text{min}$ under an argon atmosphere from $20 \text{ }^\circ\text{C}$ up to $350 \text{ }^\circ\text{C}$. The calibration of the instrument was performed with an indium standard ($T_m = 156.6 \text{ }^\circ\text{C}$, $\Delta H_m = 28.5 \text{ J/g}$) regarding its heat flow and temperature.

2.2.7. X-ray Powdered Diffraction

The structural analysis of bare quercetin together with bare and loaded particles was implemented using the X-ray diffractometer BRUKER D8 Advance (Bruker AXS GmbH, Karlsruhe, Germany). The radiation source of choice was Cu K λ 1 radiation ($\lambda = 1.5406 \text{ \AA}$). The operating conditions of the measurements were: Cu target, Ni filter, 40 kV voltage, 40 mA current, time constant $0.1 \text{ }^\circ/\text{min}$, and angular step 0.010° throughout $3\text{--}40^\circ$. The diffractograms were examined using DIFFRACT^{plus} EVA software (Bruker AXS GmbH, Karlsruhe, Germany).

2.2.8. Release Simulation of the Active Compound and Mathematical Modelling of the Process

Different quantities of the five types of quercetin-loaded complexes, all equivalent to a 10 mg mass of the active compound, were used for in vitro simulation of the release process. The required amounts were dispersed in 1 mL of phosphate buffer (pH = 5.5), mimicking skin pH, and placed into dialysis membranes (12,000 Da MWCO, Sigma, St. Louis, MO, USA). Each particle-containing membrane was placed into 20 mL of the same buffer into

a beaker containing 150 μL of TWEEN 20. These solutions were kept at 32 ± 0.5 $^{\circ}\text{C}$ and continuously stirred by a magnetic stirrer for 24 h. At chosen time frames, 3 mL of the dissolution media was taken out for spectrophotometric analysis with Metertech SP-8001 (Metertech Inc., Nangang, Taipei, Taiwan) and replenished through the addition of fresh buffer. The concentration of the collected sample was measured at 256 nm, and the amount of released quercetin was calculated using a previously determined calibration curve.

A zero-order model of release kinetics was used for fitting the experimental data.

2.2.9. Statistical Analysis

The statistical analysis and standard deviations were calculated using MS Excel (version 2016, Microsoft Corporation, Redmond, WA, USA). The drug release kinetics were fitted into a mathematical model with TableCurve™ 2D (version 5.01, Sigma-Aldrich, St. Louis, MO, USA).

3. Results and Discussion

3.1. Formation and Characterization of Casein/Chitosan Gel Polyelectrolyte Complexes

The pH level plays a crucial role in the complexation process because it regulates the degree of ionization of ionic groups and influences the intensity of the electrostatic interactions between charged components. In the present research, the pH of the synthesis medium was specifically chosen to ensure the difference in charge of the chitosan and casein molecules during the synthesis process. Due to the attractive electrostatic interaction, casein/chitosan polyelectrolyte complexes were successfully created. Based on Katchalsky's theory about weak polyelectrolytes [26], the degree of ionization of chitosan at pH 6 was calculated to be 72% and that of casein was calculated to be 94%. Therefore, both polyelectrolytes were characterized with high charge density, which causes the formulation of insoluble precipitates. Similar results were already presented by other authors [27].

The complexation process between casein and chitosan was confirmed by FT-IR analysis. The FT-IR spectra of casein, chitosan, and their complex are presented in Figure 1.

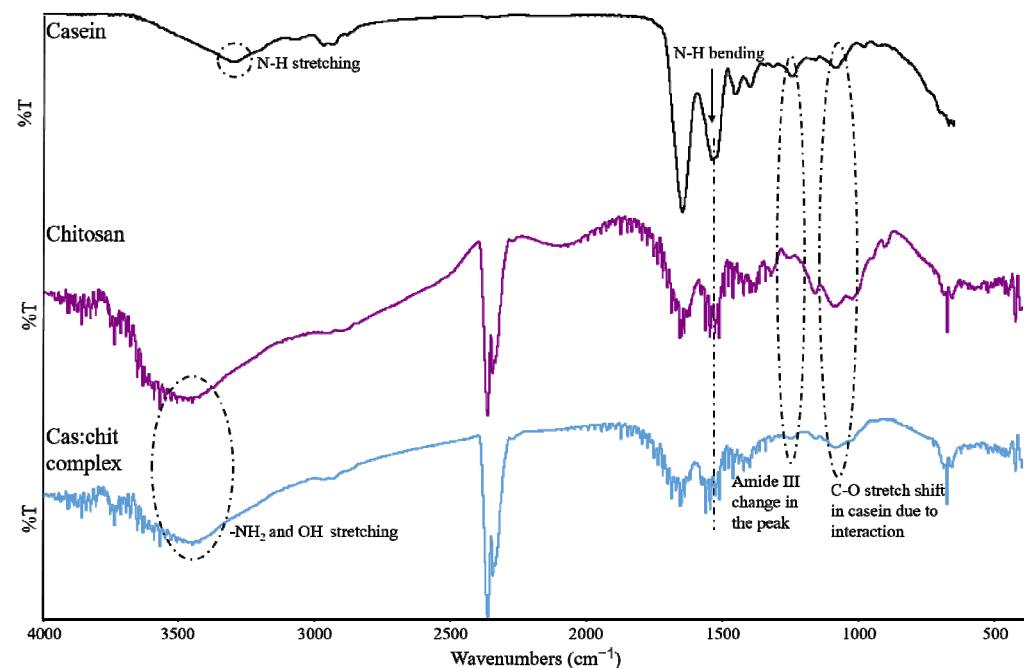


Figure 1. FT-IR spectra of casein, chitosan, and their complex at casein/chitosan charge ratio 1:1.

The spectrum of casein shows characteristic peaks at 3292 cm^{-1} , around 1550 cm^{-1} , and 1241 cm^{-1} corresponding to N-H stretching, Amide II (N-H bending and C-H stretching), and Amide III (β -sheet structure) [26]. Detected characteristic peaks for chitosan

are at 1652 cm^{-1} N-H deformation in Amide I, 1318 cm^{-1} Amide III, and 1091 cm^{-1} C-O vibration of tensional bonds [28]. Evidence for the complex formation can be found in the complexes' spectrum, showing characteristic bands of chitosan around 3500 cm^{-1} and 2359 cm^{-1} and a shift in the band of the primary amide of chitosan and the tertiary amide of casein along with a change in the peak shape and intensity around 1073 cm^{-1} [29].

The composition and some main characteristics of the gel particles are presented in Table 1.

Table 1. Size, yield, and loading efficiency of casein/chitosan gel complexes.

Sample Name	Cas [COO ⁻]/Ch[NH ₃ ⁺] Ratio *	Particle Size [nm]	Span	Yield (%)	Loading Efficiency (%)
S1	1:1	460	1.237	37.5	95.0
S2	2:1	460	7.068	43.2	95.5
S4	4:1	377	0.912	65.2	95.8
S6	6:1	5720	0.949	72.5	99.6

* The total amount of the reaction mixture is always constant and equal to 20 mL.

The casein/chitosan complexes S1, S2, and S4 were characterized as submicron structures with mean diameters of 460, 460, and 377 nm, respectively. These results demonstrate a relatively narrow monomodal size distribution in the size range between 250 and 1000 nm with a Span around 1. While samples S1, S2, and S4 do not vary greatly in size, the size of sample S6 increases sharply and shifts into the micron range ($5.720\text{ }\mu\text{m}$). For this sample, the size distribution changes to bimodal, and the Span increases to 7.068, indicating an aggregation tendency not observed in the other samples. A possible explanation for this could be related to the stabilizing role of chitosan. Casein is an amphiphilic protein with distinct hydrophobic and hydrophilic domains, which would result in the self-assembly of the casein molecules into stable micellar structures in aqueous solutions [30]. Chitosan is a hydrophilic polysaccharide and at a pH below its pKa, its primary amine groups become protonated, which would lead to the dissolution of the polysaccharide. Because of its high charge density (usually in the abovementioned conditions), the chitosan macromolecule is in a stretched conformation [31]. This way, it is located around the casein micelle and flocculates casein at low polysaccharide concentrations, while stabilizing it at moderate to high concentrations [32].

Casein/chitosan complex morphology was examined by SEM and AFM—Figures 2 and 3.

The SEM microphotograph shows gel particles with three different patterns: rough spherical particles, wrinkled spherical particles, and wrinkled irregularly shaped particles. A pronounced tendency to aggregation is noticed. Similar aggregation behaviour was observed for casein phosphopeptides–chitosan composite nanoparticles in the research of Liang et al. [33], in which the authors raise the hypothesis that highly hydrophilic chitosan packs some individual casein lamellas together and tightly adheres to their surface, forming the so-called core–shell structure. Additionally, the boundary between the individual particles is not clear, and, in places, they can even connect into one piece. In their works, other authors talk about a “hair layer,” formed by the chitosan adsorbed on the casein lamellas' surface [34].

The image from the AFM microphotograph (Figure 3a) indicates the presence of both individual spherical complexes and aggregates. After obtaining cross-section data (Figure 3b), the sizes of the casein–chitosan structures were estimated and found to be similar to the results obtained with the DLS technique.

One of the most essential characteristics of the synthesis process that determines its economic viability is its yield. Based on the data presented in Table 1, the yield of casein/chitosan formations greatly depends on the polyelectrolyte charge ratio. It is the highest for samples with an excess of casein, with 72.5% for complexes synthesized at

casein/chitosan ratio 6:1, and it then drops to 37.5% with an increase in the chitosan content. The observed trend may be related to the structure of the complex—namely, an insoluble core created from casein micelles surrounded by a loose shell of chitosan molecules [35].

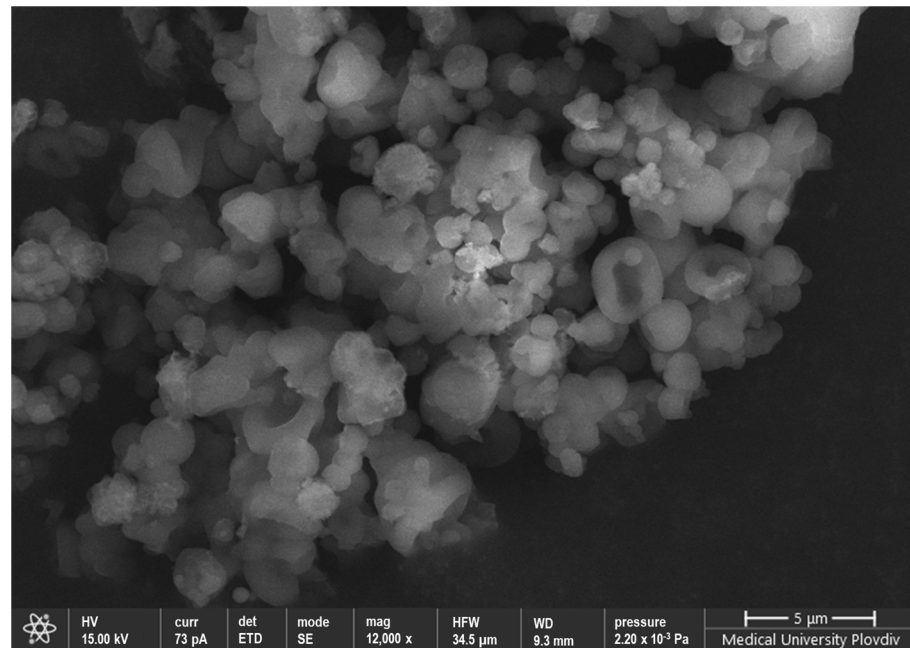


Figure 2. SEM microphotography of casein/chitosan complex (Sample S4).

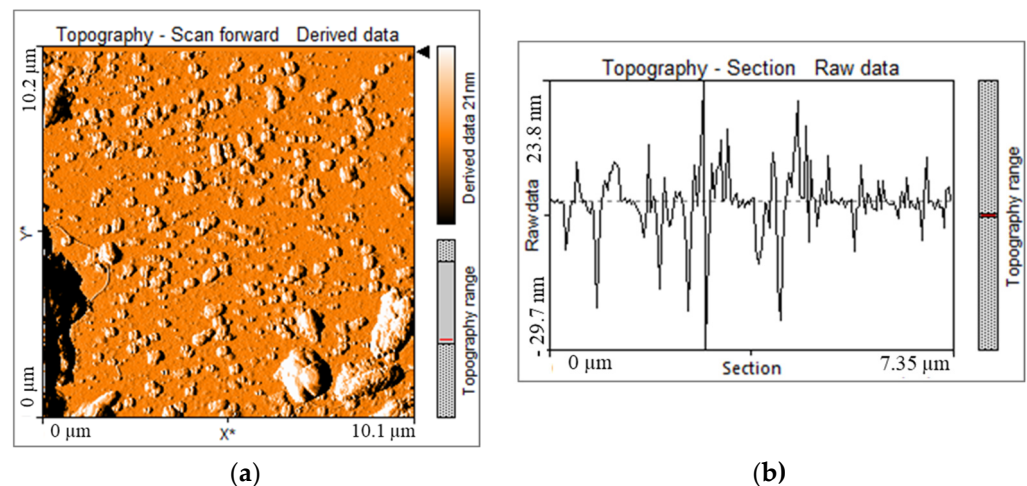


Figure 3. AFM microphotograph (a) and cross-section (b) of casein/chitosan complex (Sample S4).

3.2. Characterization of Quercetin-Loaded Casein/Chitosan Gel Polyelectrolyte Complexes

The loading of quercetin in the casein/chitosan gel particles can be proven with FT-IR spectroscopy (Figure 4). The characteristic peaks for quercetin are as follows: band in the region between 3400 cm^{-1} and 3200 cm^{-1} corresponding to —OH stretching, peak at 1664 cm^{-1} showing carbonyl group stretch in the aromatic ketone, 1611 cm^{-1} representing aromatic bending, 1214 cm^{-1} evident for the bending of the —OH groups in the phenol, and peak at 1092 cm^{-1} due to the aromatic bending [36]. The presence of the same peaks and broad bands of quercetin in the final/complex spectra confirms the presence of quercetin in the casein/chitosan complexes. Thus, it can be concluded that the substance is physically incorporated within the complexes without chemical interaction between the two. The lack of any noticeable changes in both the position and shape of the quercetin peaks can

also indicate its successful physical incorporation within the casein–chitosan network without the formation of any covalent or hydrogen bonds between the network and the incorporated substance.

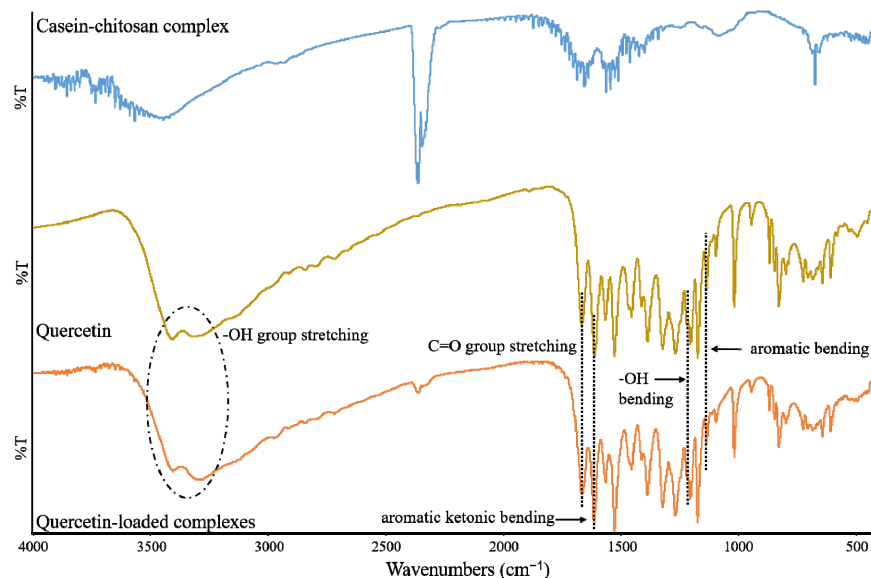


Figure 4. FT-IR spectra of neat quercetin and blank and quercetin-loaded CAS/CH gel complexes.

The loading efficiency of quercetin is very high (above 95% for all investigated samples), and it reaches a maximum value for S6 (casein/chitosan charge ratio 6:1). This behaviour is typical for hydrophobic compounds in general and for quercetin in particular. The incorporation of hydrophobic compounds in polymeric carriers is driven by the hydrophobic attractions between hydrophobic segments of the different polymers, such as the hydrophobic core of the casein micelles and the hydrophobic bioactive compounds (the polyphenol rings of quercetin) [37,38].

The amount of quercetin released in phosphate buffer at pH 5.5 and a constant temperature of 32.0 ± 0.5 °C during the first 480 min (8 h) after immersion in the medium is presented in Figure 5.

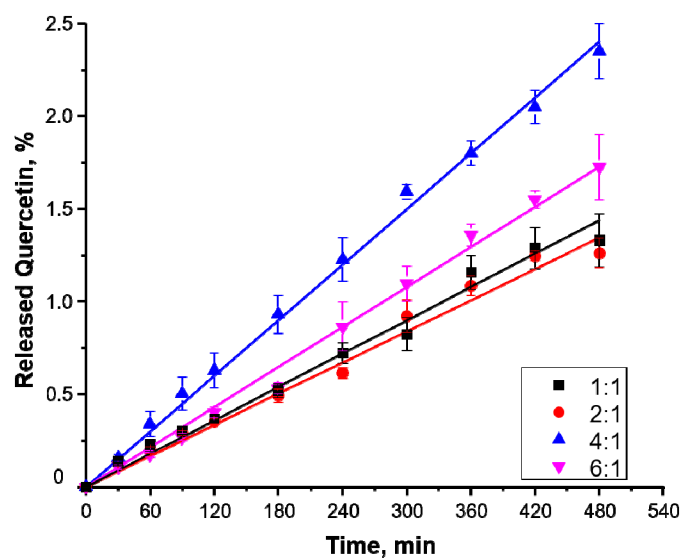


Figure 5. Quercetin release from CAS/CH complexes.

The release during the first 8 h is incomplete, varying between 1% and 2.5% depending on the complex composition. The results demonstrate no burst effect or linear release kinetics. Analogously, very slow release of quercetin from poly (lactic-co-glycolic acid) microspheres is reported by Nguyen and Jeong [39], who found that only 40% of the included drug amount is released during a month. Similar achievements were reached by Mohan and co-authors, who studied the quercetin release from TiO₂ nanotubes coated with chitosan [40]. They found about 2% release in the first 8 h. Despite the slow release rate, if we assume that the studied matrix contains 50 mg of quercetin, within 8 h, a released amount will be adequate to prevent inflammation after post-operative surgery [41].

The best fitting results of the experimental data were achieved with the zero-order kinetics model [42]:

$$Q_t = Q_0 + K_0t \quad (4)$$

where Q_t is the cumulative amount of drug released at time t , Q_0 is the initial amount of drug, K_0 is the release kinetic constant, and t is the time at which the drug release is measured. Usually, this model is applicable in core-shell systems, where a core containing the drug is surrounded by polymeric matrices. Drug release is mediated by diffusion through the surrounding polymeric matrices. Zero-order release is maintained because a constant concentration gradient of drug is kept in the polymeric matrices as long as the reservoir contains a saturated solution and sufficient excess of solid drug [43]. The observed type of release kinetics could be associated with the casein/chitosan gel polyelectrolyte complex structure, which has already been discussed.

The values of the calculated parameters of the zero-order kinetics model are presented in Table 2.

Table 2. Model parameters of the zero-order model describing the release kinetics of casein/chitosan complexes.

Sample Name	K_0 , [min ⁻¹]	DF Adj r^2	Fit SE	F-Value
S1	0.0030 ± 2.1%	0.986	0.054	758
S2	0.0028 ± 2.3%	0.984	0.054	301
S4	0.0050 ± 1.1%	0.996	0.046	3064
S6	0.0036 ± 1.6%	0.993	0.050	1512

Based on the values of the release kinetic constant, the fastest release is observed in complexes S4 (with casein/chitosan charge ratio of 4:1), followed by samples S6 (with casein/chitosan charge ratio of 6:1). The slowest release rate is observed in samples S1 and S2, whose release kinetic constant values are practically identical.

The main factors affecting the release rate are the diffusion coefficient of the drug through the carrier, the size of said carrier, and the physical state of the drug.

The faster release from the S4 gel structures may be due to their smaller size and relatively smaller amount of chitosan in comparison to samples S1 and S2, which, in aqueous medium, swell greatly and prolong the diffusion path of the drug.

As quercetin is a highly crystalline and poorly water-soluble compound, it is important to examine its phase state after it has been loaded in a drug delivery system.

Differential scanning calorimetry and the X-ray powdered diffraction technique are employed to examine its crystallinity before and after the entrapment.

The thermal stability and phase state of empty gel complexes, native quercetin, and quercetin-loaded gels have been investigated in the thermal region between room temperature and up to 350 °C (Figure 6).

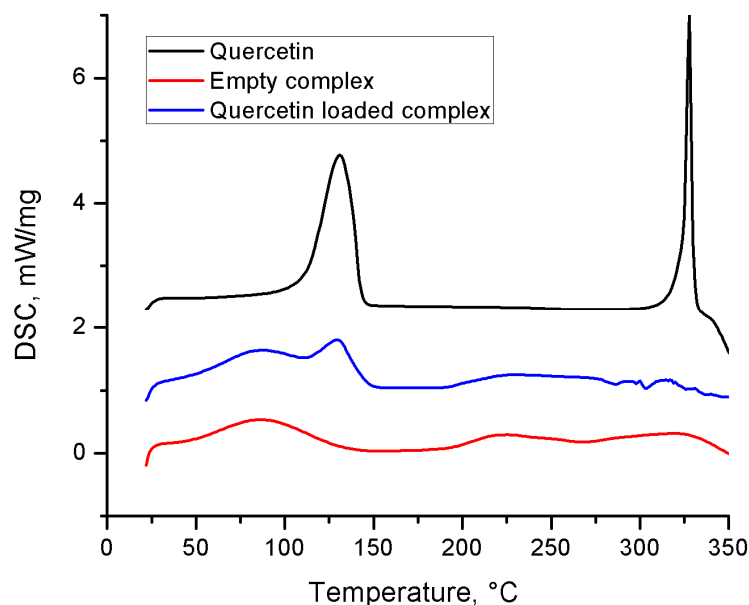


Figure 6. DSC thermograms of neat quercetin and blank and quercetin-loaded CAS/CH gel complexes for sample S4.

The DSC curve of neat quercetin indicates two endothermic events corresponding to its dehydration temperature (130 °C) and melting point (328 °C), followed by rapid decomposition. These results are confirmed by other authors [44]. DSC thermograms of blank CAS:CH gel complexes show a wide endothermic peak related to water bound in the complexes [45], but no definite peaks due to melting or degradation. The sharp peak at 328 °C indicative of melting of native quercetin is absent from the thermogram of quercetin-loaded particles, while the characteristic peak at 130 °C is still visible, proving the immobilization of the drug in the complexes. According to Tsiptsias et al. [46], this peak corresponds to the loss of endocrystalline solvent in three different polymorphs of quercetin. Transitions at temperatures around 100 °C are indicative of different thermal events, such as dehydration or glass transition, also mentioned as thermochemical transition. In the case of quercetin, the transition above 100 °C is a solid–solid thermochemical transition. Such a type of conversion is also reported for other flavanols and affects their ability to form hydrogen bonds. Vaz et al. [47] confirm this by pointing out the higher point of boiling water from the crystal lattice due to the strongly attached water molecules via hydrogen bonds to the quercetin crystals. Similar DSC thermograms were observed for all investigated samples.

The crystallinity of quercetin was qualitatively confirmed by the X-ray powdered diffraction technique (Figure 7).

Prior to loading, neat quercetin shows multiple sharp peaks in the XRPD curve due to its native crystalline state. No sharp peaks are seen in empty casein–chitosan complexes (S4) due to their amorphous nature. A significant change in the diffraction pattern is seen after quercetin incorporation into the polyelectrolyte complexes. Most of the sharp peaks can no longer be observed, but some of them are still present and slightly shifted (peak at $2\theta = 10.76^\circ$ and 31° shifted to 11.27° and 29.54° , respectively) or significantly broadened in a halo-type peak in the region $2\theta = 17\text{--}24^\circ$ [48,49]. The existence of some sharp peaks suggests that partial recrystallization phenomena occurred for the quercetin, despite obvious phase transition of its main volume. After loading quercetin into the polymer matrix, an essentially amorphous state with a broad and diffused pattern and a lack of intense peaks, unlike the diffractogram of native quercetin, was reported by Zheng et al. as well [50].

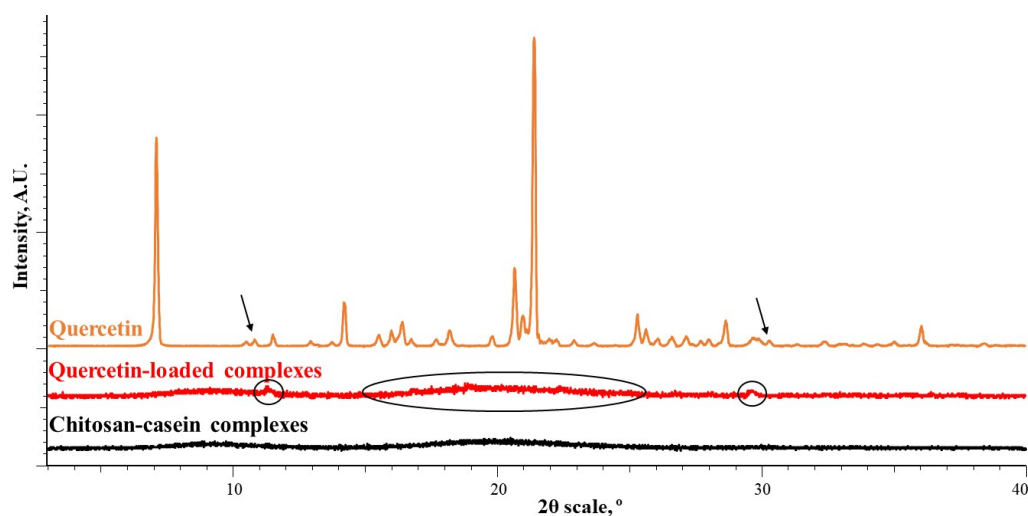


Figure 7. XRPD of neat quercetin and blank and quercetin-loaded CAS/CH gel complexes for sample S4.

4. Conclusions

In the present study, casein/chitosan gel polyelectrolyte complexes were successfully formulated to entrap quercetin using an ionotropic gelation method. It was shown that the charge ratio (respectively, the mass ratio) between polymers greatly affected the properties of the complexes. At casein/chitosan charge ratios of 1:1, 2:1, and 4:1, the complexes are nanosized with an average diameter of about 400 nm, while, with the increase in the casein excess, their sizes increase dramatically and reach several microns. The yield of the complexation is also casein/chitosan-charge-ratio-dependent and increases from 37.5% to 72.5% in excesses of casein. Due to its hydrophobicity, quercetin most probably is entrapped in the hydrophobic part of the casein micelles, with loading efficiency above 95%. It is found that the quercetin release is prolonged and carried out by a zero-order kinetic model. The release kinetics can be controlled by varying the casein/chitosan ratio. In terms of faster quercetin release, complexation yield, nanoscale size, and narrow size distribution, the model S4 (casein/chitosan charge ratio of 4:1) could be selected as the most successful.

Author Contributions: Conceptualization, M.M. and B.P.; methodology, S.M., N.Z. and R.A.; investigation, S.M., N.Z. and M.M.; data curation, M.M. and B.P.; writing—original draft preparation, S.M.; writing—review and editing, M.M. and B.P.; supervision, M.M.; project administration, M.M. and B.P. All authors have read and agreed to the published version of the manuscript.

Funding: This research received no external funding.

Institutional Review Board Statement: Not applicable.

Informed Consent Statement: Not applicable.

Data Availability Statement: Not applicable.

Acknowledgments: The authors thank the project BG05M20P001-1.002-0005, Personalized Innovative Medicine Competence Center (PERIMED), for the provided instrumentation used during this study.

Conflicts of Interest: The authors declare no conflict of interest.

References

1. Wang, L.; Dong, J.; Zhao, Z.; Li, D.; Dong, W.; Lu, Y.; Jin, B.; Li, H.; Li, H.; Liu, Q.; et al. Quarternized chitosan/quercetin/polyacrylamide semi-interpenetrating network hydrogel with recoverability, toughness and antibacterial properties for wound healing. *Int. J. Biol. Macromol.* **2023**, *228*, 48–58. [[CrossRef](#)]
2. Thangadurai, D.; Sangeetha, J.; Prasad, R. *Functional Bionanomaterials*; Springer International Publishing: Cham, Switzerland, 2020.

3. Li, Y.; Yao, J.; Han, C.; Yang, J.; Chaudhry, M.T.; Wang, S.; Liu, H.; Yin, Y. Quercetin, Inflammation and Immunity. *Nutrients* **2016**, *8*, 167. [[CrossRef](#)] [[PubMed](#)]
4. Manca, M.; Lai, F.; Pireddu, R.; Valenti, D.; Schlich, M.; Pini, E.; Ailuno, G.; Fadda, A.; Sinico, C. Impact of nanosizing on dermal delivery and antioxidant activity of quercetin nanocrystals. *J. Drug Deliv. Sci. Technol.* **2020**, *55*, 101482. [[CrossRef](#)]
5. Iweala, E.J.; Oluwapelumi, A.E.; Dania, O.E.; Ugboogu, E.A. Bioactive Phytoconstituents and Their Therapeutic Potentials in the Treatment of Haematological Cancers: A Review. *Life* **2023**, *13*, 1422. [[CrossRef](#)]
6. Wendlocha, D.; Krzykawski, K.; Mielczarek-Palacz, A.; Kubina, R. Selected Flavonols in Breast and Gynecological Cancer: A Systematic Review. *Nutrients* **2023**, *15*, 2938. [[CrossRef](#)] [[PubMed](#)]
7. Khan, K.U.; Minhas, M.U.; Badshah, S.F.; Suhail, M.; Ahmad, A.; Ijaz, S. Overview of nanoparticulate strategies for solubility enhancement of poorly soluble drugs. *Life Sci.* **2022**, *291*, 120301. [[CrossRef](#)]
8. Zaid Alkilani, A.; Hamed, R.; Abdo, H.; Swellmeen, L.; Basheer, H.A.; Wahdan, W.; Abu Kwiak, A.D. Formulation and Evaluation of Azithromycin-Loaded Niosomal Gel: Optimization, In Vitro Studies, Rheological Characterization, and Cytotoxicity Study. *ACS Omega* **2022**, *7*, 39782–39793. [[CrossRef](#)] [[PubMed](#)]
9. Bingol Ozakpinar, O.; Dastan, H.; Gurboga, M.; Sayin, F.S.; Ozsavci, D.; Caliskan Salihi, E. Carbon Nanofiber—Sodium Alginate Composite Aerogels Loaded with Vitamin D: The Cytotoxic and Apoptotic Effects on Colon Cancer Cells. *Gels* **2023**, *9*, 561. [[CrossRef](#)]
10. Anwer, M.K.; Aldawsari, M.F.; Iqbal, M.; Almutairy, B.K.; Soliman, G.A.; Aboudzadeh, M.A. Diosmin-Loaded Nanoemulsion-Based Gel Formulation: Development, Optimization, Wound Healing and Anti-Inflammatory Studies. *Gels* **2023**, *9*, 95. [[CrossRef](#)]
11. Dubey, S.K.; Dey, A.; Singhvi, G.; Pandey, M.M.; Singh, V.; Kesharwani, P. Emerging trends of nanotechnology in advanced cosmetics. *Colloids Surf. B* **2022**, *214*, 112440. [[CrossRef](#)]
12. Liu, L.; Javed, H.U.; Xiao, J. Engineering emulsion gels as functional colloids emphasizing food applications: A review. *Front. Nutr.* **2022**, *9*, 890188.
13. Mirza, M.A.; Ahmad, S.; Mallick, M.N.; Manzoor, N.; Talegaonkar, S.; Iqbal, Z. Development of a novel synergistic thermosensitive gel for vaginal candidiasis: An in vitro, in vivo evaluation. *Colloids Surf. B* **2013**, *103*, 275–282. [[CrossRef](#)] [[PubMed](#)]
14. Esposito, L.; Barbosa, A.I.; Moniz, T.; Costa Lima, S.; Costa, P.; Celia, C.; Reis, S. Design and Characterization of Sodium Alginate and Poly(vinyl) Alcohol Hydrogels for Enhanced Skin Delivery of Quercetin. *Pharmaceutics* **2020**, *12*, 1149. [[CrossRef](#)] [[PubMed](#)]
15. Rodrigues, S.; Dionísio, M.; López, C.R.; Grenha, A. Biocompatibility of Chitosan Carriers with Application in Drug Delivery. *J. Funct. Biomater.* **2012**, *3*, 615–641. [[CrossRef](#)] [[PubMed](#)]
16. Lungu, R.; Paun, M.-A.; Peptanariu, D.; Ailincăi, D.; Marin, L.; Nichita, M.-V.; Paun, V.-A.; Paun, V.-P. Biocompatible Chitosan-Based Hydrogels for Bioabsorbable Wound Dressings. *Gels* **2022**, *8*, 107. [[CrossRef](#)]
17. Karayianni, M.; Sentoukas, T.; Skandalis, A.; Pippa, N.; Pispas, S. Chitosan-Based Nanoparticles for Nucleic Acid Delivery: Technological Aspects, Applications, and Future Perspectives. *Pharmaceutics* **2023**, *15*, 1849. [[CrossRef](#)]
18. An, F.; Feng, X.; Dang, Y.; Sun, D. Enhancing nitrate removal efficiency of micro-sized zero-valent iron by chitosan gel balls encapsulating. *Sci. Total Environ.* **2022**, *823*, 153641. [[CrossRef](#)]
19. Eddin, F.B.K.; Fen, Y.W.; Sadrolhosseini, A.R.; Liew, J.Y.C.; Daniyal, W.M.E.M.M. Optical Property Analysis of Chitosan-Graphene Quantum Dots Thin Film and Dopamine Using Surface Plasmon Resonance Spectroscopy. *Plasmonics* **2022**, *17*, 1985–1997. [[CrossRef](#)]
20. Tan, Z.; Zhao, H.; Sun, F.; Ran, L.; Yi, L.; Zhao, L.; Wu, J. Fabrication of Chitosan/MXene multilayered film based on layer-by-layer assembly: Toward enhanced electromagnetic interference shielding and thermal management capacity. *Compos. A Appl.* **2022**, *155*, 106809. [[CrossRef](#)]
21. Kim, H.-S.; Park, H.; Cho, W.-J. Biocompatible Casein Electrolyte-Based Electric-Double-Layer for Artificial Synaptic Transistors. *Nanomaterials* **2022**, *12*, 2596. [[CrossRef](#)]
22. Khatun, S.; Appidi, T.; Rengan, A. Casein nanoformulations-Potential biomaterials in theranostics. *Food Biosci.* **2022**, *50*, 102200. [[CrossRef](#)]
23. Sadiq, U.; Gill, H.; Chandrapala, J. Casein Micelles as an Emerging Delivery System for Bioactive Food Components. *Foods* **2021**, *10*, 1965. [[CrossRef](#)] [[PubMed](#)]
24. Meka, V.S.; Sing, M.K.; Pichika, M.R.; Nali, S.R.; Kolapalli, V.R.; Kesharwani, P. A comprehensive review on polyelectrolyte complexes. *Drug Discov. Today* **2017**, *22*, 1697–1706. [[CrossRef](#)] [[PubMed](#)]
25. Carnal, F.; Stoll, S. Adsorption of weak polyelectrolytes on charged nanoparticles. Impact of salt valency, pH, and nanoparticle charge density. Monte Carlo simulations. *J. Phys. Chem. B* **2011**, *115*, 12007–12018. [[CrossRef](#)]
26. Panão Costa, J.; Carvalho, S.; Jesus, S.; Soares, E.; Marques, A.P.; Borges, O. Optimization of chitosan- α -casein nanoparticles for improved gene delivery: Characterization, stability, and transfection efficiency. *AAPS Pharm. Sci. Tech.* **2019**, *20*, 1–12. [[CrossRef](#)] [[PubMed](#)]
27. Dyrda-Terniuk, T.; Pryshchepa, O.; Rafińska, K.; Kolankowski, M.; Gołębiowski, A.; Gloc, M.; Dobrucka, R.; Kurzydłowski, K.; Pomastowski, P. Immobilization of silver ions onto casein. *Colloids Surf. A Physicochem. Eng.* **2023**, *667*, 131390. [[CrossRef](#)]
28. Gherman, S.P.; Biliuță, G.; Bele, A.; Ipate, A.M.; Baron, R.I.; Ochiuz, L.; Șpac, A.F.; Zavastin, D.E. Biomaterials Based on Chitosan and Polyvinyl Alcohol as a Drug Delivery System with Wound-Healing Effects. *Gels* **2023**, *9*, 122. [[CrossRef](#)]
29. Hasanvand, E.; Razavi, S.M.A. Fabrication and characterisation of milk proteins-chitosan complex coacervates. *Int. Dairy J.* **2023**, *145*, 105716. [[CrossRef](#)]

30. Elzoghby, A.O.; El-Fotoh, W.S.A.; Elgindy, N.A. Casein-based formulations as promising controlled release drug delivery systems. *JCR* **2011**, *153*, 206–216. [[CrossRef](#)]
31. Lamarque, G.; Lucas, J.M.; Viton, C.; Domard, A. Physicochemical behavior of homogeneous series of acetylated chitosans in aqueous solution: Role of various structural parameters. *Biomacromolecules* **2005**, *6*, 131–142. [[CrossRef](#)]
32. Ding, L.; Huang, Y.; Cai, X.; Wang, S. Impact of pH, ionic strength and chitosan charge density on chitosan/casein complexation and phase behavior. *Carbohydr. Polym.* **2019**, *208*, 133–141. [[CrossRef](#)]
33. Liang, Q.; Sun, X.; Raza, H.; Khan, M.A.; Ma, H.; Ren, X. Fabrication and characterization of quercetin loaded casein phosphopeptides-chitosan composite nanoparticles by ultrasound treatment: Factor optimization, formation mechanism, physicochemical stability and antioxidant activity. *Ultrason. Sonochem.* **2021**, *80*, 105830. [[CrossRef](#)] [[PubMed](#)]
34. Hu, B.; Wang, S.S.; Li, J.; Zeng, X.X.; Huang, Q.R. Assembly of bioactive peptide-chitosan nanocomplexes. *J. Phys. Chem. B* **2011**, *115*, 7515–7523. [[CrossRef](#)] [[PubMed](#)]
35. Lall, A.; Kamdem Tamo, A.; Doench, I.; David, L.; Nunes de Oliveira, P.; Gorzelanny, C.; Osorio-Madrado, A. Nanoparticles and colloidal hydrogels of chitosan-caseinate polyelectrolyte complexes for drug-controlled release applications. *Int. J. Mol. Sci.* **2020**, *21*, 5602. [[CrossRef](#)]
36. Liu, S.; Fang, Z.; Ng, K. Incorporating inulin and chitosan in alginate-based microspheres for targeted delivery and release of quercetin to colon. *Food Res. Int.* **2022**, *160*, 111749. [[CrossRef](#)]
37. Ha, H.K.; Kim, J.W.; Lee, M.R.; Lee, W.J. Formation and characterization of quercetin-loaded chitosan oligosaccharide/ β -lactoglobulin nanoparticle. *Food Res. Int.* **2013**, *52*, 82–90. [[CrossRef](#)]
38. Ghayour, N.; Hosseini, S.M.H.; Eskandari, M.H.; Esteghlal, S.; Nekoei, A.R.; Gahrue, H.H.; Tatar, M.; Naghibalhossaini, F. Nanoencapsulation of quercetin and curcumin in casein-based delivery systems. *Food Hydrocoll.* **2019**, *87*, 394–403. [[CrossRef](#)]
39. Nguyen, T.T.; Jeong, J.H. Development of a single-jet electrospray method for producing quercetin-loaded poly (lactic-co-glycolic acid) microspheres with prolonged-release patterns. *J. Drug Deliv. Sci. Technol.* **2018**, *47*, 268–274. [[CrossRef](#)]
40. Mohan, L.; Anandan, C.; Rajendran, N. Drug release characteristics of quercetin-loaded TiO₂ nanotubes coated with chitosan. *Int. J. Biol. Macromol.* **2016**, *93*, 1633–1638. [[CrossRef](#)]
41. Urmila, J.; Joshi, S.; Amol, G.; D’Mello, P.; Sinha, R.; Srivastava, S.; Govil, G. Anti-inflammatory, antioxidant and anticancer activity of Quercetin and its analogues. *Inter. J. Res. Pharm. Biomed. Sci.* **2011**, *2*, 1756–1766.
42. Peek, C.R.; Middaugh, C.; Berkland, C. Nanotechnology in vaccine delivery. *Adv. Drug Deliv. Rev.* **2008**, *60*, 915–928. [[CrossRef](#)] [[PubMed](#)]
43. Yoshida, R.; Sakai, K.; Okano, T.; Sakurai, Y. A new model for zero-order drug release I. Hydrophobic drug release from hydrophilic polymeric matrices. *Polym. J.* **1991**, *23*, 1111–1121. [[CrossRef](#)]
44. Li, X.Y.; Li, Y.C.; Yu, D.G.; Liao, Y.Z.; Wang, X. Fast disintegrating quercetin-loaded drug delivery systems fabricated using coaxial electrospinning. *Int. J. Mol. Sci.* **2013**, *14*, 21647–21659. [[CrossRef](#)] [[PubMed](#)]
45. Karki, R.; Joshi, H.; Divakar, G. Fabrication of Casein-chitosan Microparticles of Curcumin for Controlled Delivery-Physicochemical Characterization. *Micro Nanosyst.* **2017**, *9*, 88–96.
46. Tsiptsias, C.; Tsvintzelis, I. On the Thermodynamic Thermal Properties of Quercetin and Similar Pharmaceuticals. *Molecules* **2022**, *27*, 6630. [[CrossRef](#)]
47. Vaz, G.R.; Clementino, A.; Bidone, J.; Villetti, M.A.; Falkembach, M.; Batista, M.; Barros, P.; Sonvico, F.; Dora, C. Curcumin and Quercetin-Loaded Nanoemulsions: Physicochemical Compatibility Study and Validation of a Simultaneous Quantification Method. *Nanomaterials* **2020**, *10*, 1650. [[CrossRef](#)]
48. Wang, W.; Liu, Y.; Zhang, H.; Ling, D.; Yan, Q.; Wu, Y.; Jin, Y.; Xie, F. Preparation of inhalable quercetin- β -cyclodextrin inclusion complexes using the supercritical antisolvent process for the prevention of smoke inhalation-induced acute lung injury. *J. CO₂ Util.* **2023**, *69*, 102414. [[CrossRef](#)]
49. Qiu, C.; Zhang, Z.; Li, X.; Sang, S.; McClements, D.J.; Chen, L.; Long, J.; Jiao, A.; Xu, X.; Jin, Z. Co-encapsulation of curcumin and quercetin with zein/HP- β -CD conjugates to enhance environmental resistance and antioxidant activity. *NPJ Sci. Food* **2023**, *7*, 29. [[CrossRef](#)]
50. Zheng, Y.; Chow, A. Production and characterization of a spray-dried hydroxypropyl- β -cyclodextrin/quercetin complex. *Drug Dev. Ind. Pharm.* **2009**, *35*, 727–734. [[CrossRef](#)]

Disclaimer/Publisher’s Note: The statements, opinions and data contained in all publications are solely those of the individual author(s) and contributor(s) and not of MDPI and/or the editor(s). MDPI and/or the editor(s) disclaim responsibility for any injury to people or property resulting from any ideas, methods, instructions or products referred to in the content.